Adsorption (2012) 18:87–102
DOI 10.1007/s10450-012-9384-4

Numerical study of nitrogen desorption by rapid oxygen purge for a medical oxygen concentrator

Siew Wah Chai · Mayuresh V. Kothare · Shivaji Sircar

Received: 18 August 2011 / Accepted: 16 April 2012 / Published online: 5 May 2012

Abstract Efficient desorption of selectively adsorbed N_2 from air in a packed column of LiX zeolite by rapidly purging the adsorbent with an O_2 enriched gas is an important element of a rapid cyclic pressure swing adsorption (RPSA) process used in the design of many medical oxygen concentrators (MOC). The amount of O_2 purge gas used in the desorption process is a sensitive variable in determining the overall separation performance of a MOC unit. Various resistances like (a) adsorption kinetics, (b) column pressure drop, (c) non-isothermal column operation, (d) gas phase mass and thermal axial dispersions, and (e) gas-solid heat transfer kinetics determine the amount of purge gas required for efficient desorption of N_2. The impacts of these variables on the purge efficiency were numerically simulated using a detailed mathematical model of non-isothermal, non-isobaric, and non-equilibrium desorption process in an adiabatic column.

The purge gas quantity required for a specific desorption duty (fraction of total N_2 removed from a column) is minimum when the process is carried out under ideal, hypothetical conditions (isothermal, isobaric, and governed by local thermodynamic equilibrium). All above-listed non-idealities (a–e) can increase the purge gas quantity, thereby, lowering the efficiency of the desorption process compared to the ideal case. Items (a–c) are primarily responsible for inefficient desorption by purge, while gas phase mass and thermal axial dispersions do not affect the purge efficiency under the conditions of operation used in this study.

Smaller adsorbent particles can be used to reduce the negative effects of adsorption kinetics, especially for a fast desorption process, but increased column pressure drop adds to purge inefficiency. A particle size range of ∼300–500 μm is found to require a minimum purge gas amount for a given desorption duty. The purge gas requirement can be further reduced by employing a pancake column design (length to diameter ratio, $L/D < 0.2$) which lowers the column pressure drop, but hydrodynamic inefficiencies (gas mal-distribution, particle agglomeration) may be introduced. Lower L/D also leads to a smaller fraction of the column volume that is free of N_2 at the purge inlet end, which is required for maintaining product gas purity.

The simulated gas and solid temperature profiles inside the column at the end of the rapid desorption process show that a finite gas-solid heat transfer coefficient affects these profiles only in the purge gas entrance region of the column. The profiles in the balance of the column are nearly invariant to the values of that coefficient. Consequently, the gas-solid heat transfer resistance has a minimum influence on the overall integrated N_2 desorption efficiency by O_2 purge for the present application.

Keywords Desorption by purge · Medical oxygen concentrator · Model simulation · Non-isothermal · Non-isobaric · Non-equilibrium

1 Introduction

Production of 90+% O_2 enriched air from ambient air by cyclic pressure swing adsorption (PSA) processes employing a N_2 selective zeolite as the adsorbent and a total cycle time of ∼30–240 seconds is a commercial technology in the tonnage-scale production [∼1–150 tons per day of contained O_2 (TPD_c)] (Sircar et al. 1999; Chai et al. 2011). A special application of this technology employing a very

S.W. Chai · M.V. Kothare · S. Sircar (✉)
Department of Chemical Engineering, Lehigh University, Bethlehem, PA 18015, USA
e-mail: sircar@aol.com

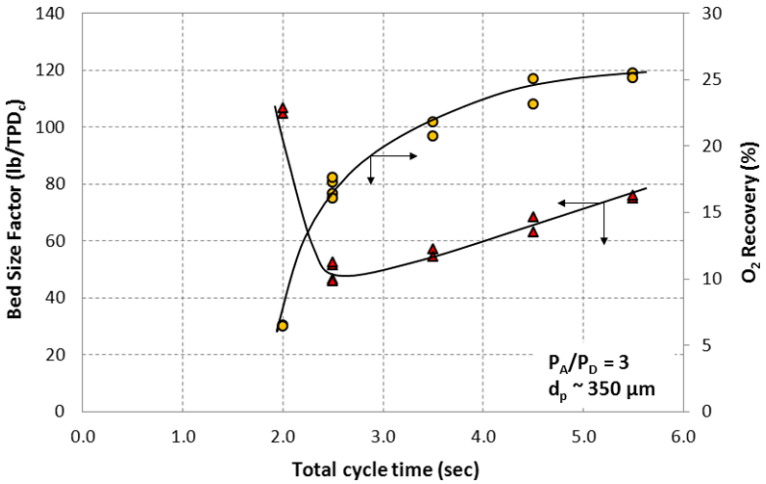

Fig. 1 Experimental RPSA process performance data for a simulated MOC using LiX zeolite

rapid pressure swing adsorption (RPSA) concept is a medical oxygen concentrator (MOC) which produces only 1–10 standard liters/minute (SLPM) of 90+% enriched O_2 for individual breathing purposes. The process cycle times used in a RPSA process are typically less than 10 seconds for reducing the adsorber sizes and thus, achieving system compactness. A summary of experimentally measured as well as model simulated performances of various RPSA MOC concepts can be found in a recent publication (Chai et al. 2011). These units typically use a LiX zeolite which is the currently preferred zeolitic adsorbent for air separation (Sircar and Myers 2003).

The RPSA process cycles used in the design of MOC are often similar to or variations of the classic Skarstrom (1960) PSA cycle where N_2 is selectively adsorbed from a stream of compressed air by flowing it over a packed column of zeolite, thereby producing the O_2 enriched product gas, followed by periodic desorption of N_2 by pressure reduction of the column and ambient-pressure back purge with a part of the O_2 enriched product gas. The N_2-enriched effluents from the desorption steps are wasted.

The back purge step is critical for a PSA process design because (a) it provides an efficient means of overall column regeneration (desorption of N_2) and (b) it creates a section of the column at the O_2 product end which is equilibrated with the O_2 enriched product gas at the start of an adsorption step. Goal (b) is critical for maintaining the product O_2 purity during the adsorption step. The two key performance variables for a PSA O_2 generator are (i) bed size factor (BSF, total amount of zeolite adsorbent in the PSA system per unit amount of contained O_2 in product gas per unit time) and (ii) net O_2 recovery by the process (R, amount of O_2 in product gas per unit amount of O_2 in feed air per cycle).

A recent experimental study of a simulated, four-step Skarstrom-like RPSA cycle for MOC application using a commercial sample of LiX zeolite and dry and CO_2-free compressed air feed, showed that there can be an optimum cycle time for the RPSA process where the BSF is lowest (smallest adsorber size) and the O_2 recovery is moderate (Chai et al. 2011). Figure 1 provides an example of such optimum RPSA process performance from that study using an adsorption pressure $P_A = 3$ atm, a desorption pressure $P_D = \sim 1$ atm and an adsorbent particle size $d_p = \sim 350$ µm. The optimum cycle time was ~2–4 seconds, the optimum BSF was ~50 lbs/TPD$_c$, and the O_2 recovery was ~20 %. Consequently, the optimum duration of a back purge step of a RPSA process for MOC needs to be <1–3 seconds, and the purge gas flow rate can be high.

The following idealized model calculation estimates the sensitivity of the specific amount of back purge gas (moles/kg of sorbent) used in a generic Skarstrom-like PSA cycle in determining *BSF* and *R*.

1.1 Sensitivity of back purge gas quantity to PSA process performance

We consider an ideal, hypothetical PSA process which produces pure O_2 from a compressed air stream consisting of 79 % N_2 + 21 % O_2 only. The cyclic process steps are: (A) counter-current column back purge at ambient pressure using pure O_2, (B) counter-current column pressurization from ambient to adsorption pressure level of P_A with pure O_2, (C) co-current adsorption from compressed air at pressure P_A to produce a pure O_2 effluent gas at pressure P_A, and (D) counter-current column depressurization from pressure P_A to ambient pressure. A part of the effluent gas from step C is withdrawn as the net pure O_2 product by the process and the balance is used in steps A and B. The effluent gases from steps A and D are wasted. Other model assumptions for the hypothetical process include (a) isothermal operation, (b) local thermodynamic equilibrium (mass and heat) between the gas and solid phases in the column at all times during the cycle, and (c) plug flow of gas with no column pressure drop or axial dispersion.

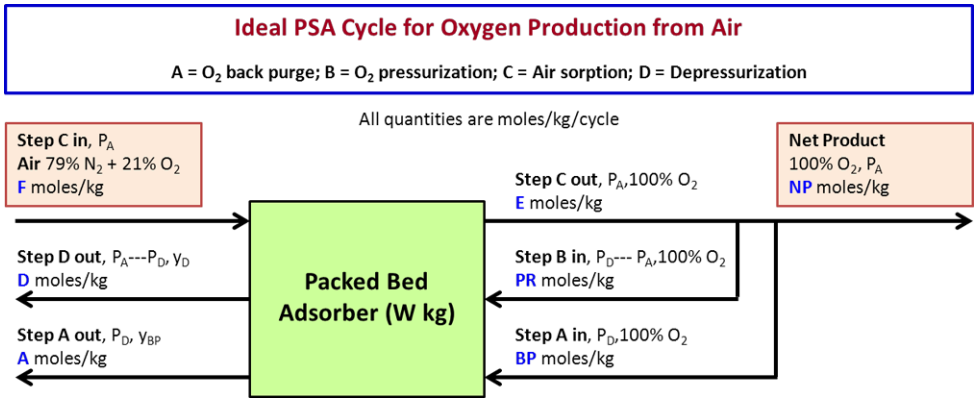

Fig. 2 Block diagram of an ideal O_2 PSA system

Figure 2 is a block diagram of the model PSA concept showing various influent and effluent flows and quantities (moles/kg of total adsorbent in the PSA system/cycle) for the steps. The key performance variables for the process are:

$$BSF = 1/(NP \cdot \omega) \tag{1}$$

$$R = NP/0.21F \tag{2}$$

where ω $(= 1/t_c)$ is the cycle frequency (number of cycles per unit time) and t_c is the total cycle time. It can be shown by component mass balances ($N_2 = 1$; $O_2 = 2$) for various steps that:

$$F = N_1^C/0.79 \tag{3}$$

$$PR = \left(N_2^B - N_2^A\right) \tag{4}$$

$$E = PR + BP + NP = 0.21F + \left(N_2^B - N_2^C\right) \tag{5}$$

$$NP = (\alpha - BP); \quad \alpha = (E - PR) \tag{6}$$

where N_i^j $[= n_i^j + \varepsilon\rho_g^j y_i^j/\rho_b]$ is the total (adsorbed + void gas) specific amount (moles/kg) of component i in the column at the end of step j, n_i^j is the specific equilibrium amount (moles/kg) of component i adsorbed at the end of step j when the gas phase density (moles/cm^3) is ρ_g^j $(= P^j/R_g T)$ and the gas phase mole fraction of component i is y_i^j. P^j (atm) is the column pressure at the end of step j, ε is the helium void fraction of the column, T is the system temperature, R_g is the gas constant, and ρ_b is the bed density. Variables F, E, PR and α can be estimated using (3)–(6) and the adsorption isotherms of pure N_2 and O_2 and their mixtures at T.

It follows from (1), (2), and (6) that:

$$\left|\frac{\Delta BSF}{BSF}\right| = \left|\frac{\Delta R}{R}\right| = \beta\left[\frac{\Delta BP}{BP}\right] \tag{7}$$

$$\beta = \left[\frac{\alpha}{0.21F(R)} - 1\right] \tag{8}$$

Equations (7) and (8) indicate that the changes in the values of the parameters (BSF) and (R) due to a change in the value of (BP) will be magnified by a factor of β (>1). Thus, the amount of back purge used in a PSA process is a sensitive variable for determining the overall performance of a PSA process.

We used the published adsorption isotherms of pure N_2 and O_2 and their mixtures on a sample of ~100 % Li exchanged X zeolite, which could be described by an empirical Langmuir-like model (Rege and Yang 1997), in order to derive the following relationship between the parameters β and R for the above-described PSA cycle by assuming that the adsorption pressure (P_A) is 5 atm and the system temperature (T) is 298 K:

$$\beta = \left[\frac{1.31}{R} - 1\right] \tag{9}$$

According to (9), the value of the parameter β is 4.24 if the base case O_2 recovery is 25 % $(R = 0.25)$, which is typical for an O_2 RPSA system (Chai et al. 2011). Consequently, it follows from (7) and (9) that a ~10 % change (or estimation error) in the quantity of back purge (BP) from a base case value can produce a ~42.4 % change (or estimation error) in BSF or R from those of the base case values. This simplified, ideal model performance evaluation clearly demonstrates that the quantity of back purge in a PSA process is a very sensitive design variable in establishing the overall process performance, and the effects of different non-idealities such as mass, heat, and momentum transfer resistances present in a real PSA process on the purge gas requirement must be considered for a meaningful PSA process design.

1.2 Traditional assumptions used in modeling rapid PSA process concepts

Unfortunately, published literature on rapid PSA models often ignore the effects of these resistances as shown by Table 1, which is reproduced from an earlier publication (Chai et al. 2011). This table summarizes the key assumptions used in several numerical models of cyclic PSA O_2 processes for MOC application, where desorption of N_2 from

Table 1 Model simulation studies of various PSA O_2 concentrators

Authors	Performance			Mass transfer kinetics	Heat balance	Pressure drop	Mass axial dispersion	Adsorption isotherms	Adsorbent	Total cycle time (s)
	% O_2	Rec (%)	BSF (Ib/TPD$_c$)							
Kopaygorodsky et al. (2004) Process: RPSA $P_A = 1.6$ atm $P_D = 1.0$ atm	85	56	14.2	No resistance	No	Yes	Yes	Linear	5A zeolite monolith $d_p = 2$ μm	3
Santos et al. (2004) Process: PSA $P_A = 3.0$ atm $P_D = 1.0$ atm	94.5	22	528	LDF model	No	No	Yes	Langmuir-Freundlich	Oxysiv 5 (NaX zeolite) $d_p = \sim$600 μm	18
Santos et al. (2006) Process: PSA $P_A = 3.0$ atm $P_n = 1.0$ atm	94.5	32	455	LDF model	No	No	Yes	Langmuir-Freundlich	Oxysiv 5 (NaX zeolite) $d_p = \sim$600 μm	16
Zhong et al. (2010) Process: RPVSA $P_A = 1.5$ atm $P_0 = 0.5$ atm	90	25–50	<50	Solid phase diffusion model	Yes	Yes	Yes	Langmuir	LiX 2.0 C.D. zeolite 150 < d_p < 350 μm	<4
Rama Rao et al. (2010) Process: Pulsed PSA $P_A = 3.5$ atm $P_D = 1.0$ atm	~90	24	5.2	LDF model	No	Yes	Yes	Langmuir	Ag-Li-X zeolite $d_p = 20$ μm	0.235

a zeolite adsorbent column by purge with an O_2 enriched gas was employed as an integral part of the process. It may be seen that all of these simulations have been carried out under isothermal process conditions, except that of Zhong et al. (2010), with or without inclusion of column pressure drop in the model, and for one case, by assuming an unrealistic linear adsorption isotherm model with no adsorbate mass transfer resistances (Kopaygorodsky et al. 2004). Thus, these studies may not be rigorous enough to accurately estimate the performance of a 'desorption by purge' step used in the processes.

1.3 Model studies of desorption by purge process

It should also be mentioned that many model studies of isobaric and isothermal (or adiabatic) desorption of a single or binary adsorbates (dilute or bulk) from a packed adsorbent column by purge with a less strongly adsorbed gas (pure or binary) under the conditions of local thermodynamic equilibrium (mass and heat) have been published (Wicke 1939a, 1939b; Rhee and Amundson 1970; Rhee et al. 1972; Basmadjian et al. 1975a, 1975b; Jacob and Tondeur 1983; Sircar and Kumar 1985; Sircar and Golden 1995). A rigorous analytical solution of an isothermal and isobaric desorption by purge model for a bulk binary Langmuirian adsorbate system has also been published (Sircar and Golden 1995). It has been observed that the assumption of local equilibrium is generally adequate to describe isothermal and isobaric desorption (no column pressure drop) by purge when a low to moderate purge gas flow rate is used.

1.4 Goals of the present work

The purpose of this work is to numerically investigate the effects of various resistances in mass, heat and momentum transfer processes present inside a real packed bed adsorber undergoing a rapid 'desorption by purge' process having a duration of only a few seconds. The effects are magnified due to the shortness of the process step time. The investigation is carried out in a systematic and progressive manner in order to appreciate the relative contributions of various resistances. The study also examines the influence of adsorbent particle size and length to diameter ratio of the adsorber on the efficiency of 'desorption by purge' process.

Only a simplified desorption process where an adsorbent column packed with LiX zeolite and equilibrated with synthetic air (79 % N_2 + 21 % O_2 at 1 atm and 298 K) which is desorbed by purging with pure O_2 at 298 K is considered in the study. No attempt is made to simulate a complete PSA cycle for air separation. The rationale for such choice is that the simplified study would provide better insights on the influences of various non-idealities on the efficiency of the N_2 desorption process. The effects are complex and interactive. Uncoupling the effects of these resistances on the purge pro-

cess from the overall performance of a PSA process may not be practical.

Analysis of the effects of (a) finite ad(de)sorption mass transfer resistance, (b) column pressure drop, (c) non-isothermal desorption, (d) gas-solid heat transfer resistance, (e) gas phase mass and heat axial dispersions, (f) adsorbent particle size, (g) column length to diameter ratio, and (h) desorption time on the efficiency of the overall desorption process is carried out vis a vis an ideal (most efficient) 'desorption by purge' process which is isothermal, isobaric, and where local thermodynamic equilibrium prevails.

2 Mathematical model

The mathematical model for numerical simulation of the 'desorption by purge' process is formulated by a set of partial differential equations (PDE) which describe (a) gas and adsorbed phase mass balances for each component ($1 = N_2$; $2 = O_2$) of the gas mixture of interest, (b) gas and solid phase energy balances, and (c) the column pressure drop. They are given below in (10)–(14):

Gas phase mass balance for component i:

$$\varepsilon \frac{\partial}{\partial t}[y_i \rho_g] = -\frac{\partial}{\partial z}[Q y_i] - \rho_b \frac{\partial n_i}{\partial t} + \bar{\varepsilon} D_L \frac{\partial^2}{\partial z^2}[y_i \rho_g] \tag{10}$$

Adsorbed phase mass balance for component i (LDF model):

$$\frac{\partial n_i}{\partial t} = k_i \left[n_i^{\infty} - n_i \right] \tag{11}$$

Gas phase heat balance:

$$\varepsilon C_g \frac{\partial}{\partial t}[\rho_g \theta_g] = -C_g \frac{\partial}{\partial z}[Q \theta_g] + ha(T_s - T_g) + \bar{\varepsilon} C_g D_g \frac{\partial^2}{\partial z^2}[\rho_g \theta_g]$$

$$\theta_g(z,t) = (T_g - T_0) \tag{12}$$

Solid phase heat balance:

$$\rho_b C_s \frac{\partial}{\partial t}[\theta_s] = \rho_b \sum q_i \frac{\partial n_i}{\partial t} - ha(T_s - T_g)$$

$$\theta_s(z,t) = (T_s - T_0) \tag{13}$$

Column pressure drop (Ergun 1952):

$$\left(\frac{\partial P}{\partial z}\right)_t = -\frac{150\mu}{d_p^2 \rho_g} \frac{(1-\bar{\varepsilon})^2}{\bar{\varepsilon}^3} Q - \frac{1.75 M_g}{d_p \rho_g} \frac{(1-\bar{\varepsilon})}{\bar{\varepsilon}^3} Q^2 \tag{14}$$

where the variables $y_i(z,t)$ and $n_i(z,t)$ are, respectively, the gas phase mole fractions and adsorbed phase loadings of component i at distance z $(0 \le z \le L)$ in the adsorbent column of length L and diameter D at time t. $n_i^{\infty}(z,t)$ is the equilibrium amount of component adsorbed under the local gas phase conditions at z and t. The parameters $Q(z,t)$, $P(z,t)$, and $\rho_g(z,t)$ $[= P/RT_g]$ are, respectively, the gas phase mass flux (based on empty cross-section area, A $[= (\pi/4)D^2]$, of the adsorber), gas pressure, and gas density at z and t. $T_s(z,t)$ and $T_g(z,t)$ are respectively, the solid and gas phase temperatures at z and t. T_o is the initial column as well as the purge gas inlet temperature. k_i is the linear driving force (LDF) mass transfer coefficient for adsorbate i. h is the gas-solid heat transfer coefficient, and a $[= 6(1-\bar{\varepsilon})/d_p]$ is the effective surface area per unit column volume for gas-solid heat transfer. D_L and D_g $[= k_g/\rho_g C_g]$ are, respectively, the gas phase effective mass and heat axial dispersion coefficients. k_g, μ_g, C_g and M_g are, respectively, the gas phase thermal conductivity, viscosity, heat capacity, and molecular weight. ε, $\bar{\varepsilon}$, ρ_b, and d_p are, respectively, the helium void fraction, inter-particle void fraction, adsorbent bulk density, and adsorbent particle diameter in the column. R is the gas constant.

The key features of the proposed model are (a) inclusion of mass and heat axial dispersions in the gas phase, (b) inclusion of gas-solid heat transfer resistance, (c) exclusion of axial conduction of heat in the solid phase, (d) use of differential form of Ergun equation to describe local pressure drop in the column, and (e) use of linear driving force model to describe the overall adsorption kinetics. Other important model assumptions are (a) adiabatic column behavior, (b) absence of radial gradients inside the column, and (c) absence of gas mal-distribution or particle agglomeration.

The initial and boundary conditions used for numerical solution of the model for desorption by purge are summarized below:

$$y_1(z,0) = 0.79; \qquad y_2(z,0) = 0.21;$$
$$y_1(L,t) = 0; \qquad y_2(L,t) = 1.0 \tag{15}$$

$$P(z,0) = 1 \text{ atm}; \tag{16}$$
$$P(L,t) = P_L(t); \qquad P(0,t) = 1 \text{ atm}$$

$$\theta_g(z,0) = \theta_s(z,0) = 0; \qquad \theta_g(L,t) = 0 \tag{17}$$

$$\varepsilon C_g \frac{\partial}{\partial t}[\rho_g \theta_g] = -C_g \frac{\partial}{\partial z}[Q \theta_g] + ha(T_s - T_g)$$
$$\text{at } z = 0 \text{ for all } t \tag{18}$$

$$\varepsilon \frac{\partial}{\partial t}[y_i \rho_g] = -\frac{\partial}{\partial z}[Q y_i] - \rho_b \frac{\partial n_i}{\partial t}$$
$$\text{at } z = 0 \text{ for all } t \tag{19}$$

Where $P_L(t)$ is the inlet pressure of purge gas at time t so that the purge effluent gas pressure $[P(0,t)]$ is always 1 atm. The last two boundary conditions ((18) and (19)) are based on a proposal by Schiesser (1996) for minimum reduction

of the PDE and subsequent stability of the numerical solutions. They were used in place of the conventional Wilhelm-Wehner-Danckwerts boundary conditions $\frac{\partial}{\partial z}[\theta_g] = 0$ and $\frac{\partial}{\partial z}[y_i] = 0$ at $z = 0$ for all t which is physically unrealistic.

We used the following published correlations for estimation of adsorption equilibria (n_i^{∞}), LDF mass transfer coefficients (k_i), gas phase mass axial dispersion coefficient (D_L), and gas-solid heat transfer coefficient (h) which are input variables in the model.

Adsorption equilibria (Rege and Yang 1997):

$$n_i^{\infty} = \frac{K_i P y_i}{1 + \sum B_j P y_j}; \qquad K_i = K_i^o \exp\left[\frac{Q_{Ki}}{RT_s}\right]; \qquad B_i = B_i^o \exp\left[\frac{Q_{Bi}}{RT_s}\right] \tag{20}$$

Equation (20) is an empirical model for calculating pure and mixed gas equilibrium adsorption isotherms for N_2 and O_2 adsorption on LiX zeolite at different temperatures. The Henry's Law selectivity of adsorption of N_2 over O_2 at 298 K is 7.53 and the corresponding isosteric heats of adsorption of N_2 and O_2 are, respectively, 4.88 and 4.10 kcal/mole.

LDF mass transfer coefficients (Todd and Webley 2006; Alpay et al. 1994):

$$k_i = \frac{60 D_i^e}{d_p^2} \qquad D_i^e = \frac{\varepsilon_p}{\tau_p}\left(\frac{1}{\frac{1}{D_{K,i}^e} + \frac{1}{D_{m,1-2}^e}}\right) \tag{21}$$

where D_i^e is the effective intra particle diffusivity of component i into the adsorbent particle. $D_{K,i}^e$ and $D_{m,1-2}^e$ are effective Knudsen and molecular diffusivity of component i into the adsorbent pore. ε_p and τ_p are, respectively, the particle void fraction and particle tortuosity factor.

Mass axial dispersion coefficient (Langer et al. 1978; Ruthven 1984):

$$D_L = 0.7 D_{m,1-2}^e + \frac{0.5 d_p Q}{\bar{\varepsilon} \rho_g} \tag{22}$$

We choose (22) for estimation of D_L for all particle sizes in our work because it is traditionally used even for smaller particles (Rama Rao et al. 2010; Santos et al. 2004). A different particle size dependence of D_L for smaller particles ($d_p < 0.3$ cm) due to particle agglomeration has been correlated (Ruthven 1984). However, it can be shown that this correlation leads to a larger but particle size independent value for D_L than that by (22). Particle agglomeration is a complex and system dependent (adsorber design, particle size and shape distribution, etc.) issue which may not be easily modeled. This justifies the use of (22) for an order of magnitude estimation of D_L.

Gas-solid heat transfer coefficient:

Model studies have indicated that a finite gas-solid heat transfer resistance can substantially influence the column dynamics of adsorption (Kumar and Sircar 1984a, 1984b) as well as the separation efficiency of a rapid differential PSA system (Sircar 2005). The authors are unaware of any study of the influence of h on the efficiency of desorption by purge.

Different empirical correlations between the Nusselt number [$Nu = hd_p/k_g$] and the Reynolds number [$Re = Qd_p/\mu_g$] for calculation of h in a packed bed can be found in the literature. They differ depending on whether or not the thermal axial dispersion is included in the gas phase heat balance equation. Omission of gas phase thermal axial dispersion in a packed column apparently leads to a very low value of Nu in the low Re (< 5) region (Wakao et al. 1979; Dhingra et al. 1984). The following correlations were used in this work:

Correlation with gas phase thermal axial dispersion (Wakao et al. 1979):

$$Nu = 2.0 + 1.1 Pr^{1/3} Re^{0.6}; \quad 15 \le Re \le 8500 \tag{23}$$

Correlation without gas phase thermal axial dispersion (Kunii and Suzuki 1967):

$$Nu = 0.032[Pr \times Re]^{1.5} \tag{24}$$

The variable $Pr[= C_g \mu_g / k_g]$ in (23) and (24) is the Prandtl number. Equation (23) or (24) can be used to estimate the gas-solid heat transfer coefficient as functions of d_p [$h = k_g Re(Q, d_p)/d_p$] for a given gas mass flow rate.

Dynamic mass balance:

The total specific amount (adsorbed + void gas) of component i [$\bar{n}_i(z,t)$, moles/kg] in the column at any z and t is given by:

$$\bar{n}_i(z,t) = n_i(z,t) + \varepsilon y_i(z,t) \rho_g(z,t)/\rho_b \tag{25}$$

Overall mass balances:

The total initial specific amount of component i in the column at the start of the purge process [N_i^0, moles/kg] is given by:

$$N_i^0 = n_i^0 + \varepsilon y_i^0 \rho_g^0 / \rho_b \tag{26}$$

where superscript zero defines the uniform condition present in the column at the start of the purge process.

The total specific amount of N_2 (component 1) desorbed from the column during the purge process at time t [$N_1(t)$, moles/kg] is given by:

$$N_1(t) = \frac{1}{L\rho_b}\int_0^t Q(0,t)\,y_1(0,t)\,dt \tag{27}$$

The total residual specific amount of N_2 in the column at time t [$N_1^R(t)$, moles/kg] is given by:

$$N_1^R(t) = N_1^0 - N_1(t) = \frac{1}{L}\int_0^L \bar{n}_1(z,t)\,dz \tag{28}$$

The total specific amount of O_2 (component 2) purge gas used at time t [$\bar{Q}_2(t)$, moles/kg] is given by:

$$\bar{Q}_2(t) = \frac{1}{L\rho_b}\int_0^t Q(L,t)\,y_2(L,t)\,dt \tag{29}$$

Key performance variables for desorption process:

The key variables describing the performance of the desorption process are (a) the fraction of total N_2 initially present in the column (adsorbed + void gas) that is desorbed at time t [$f_1 = N_1(t)/N_1^0$] and (b) the fraction of column volume at the purge inlet end which is free of N_2 [F], as functions of the specific purge gas quantity at time t [$\bar{Q}_2(t)$]. Efficient desorption of N_2 by O_2 purge is represented by larger values of f_1 and F and smaller amount of $\bar{Q}_2$ at the end of the purge process.

3 Numerical simulations

The above described mathematical model for simulation of desorption by purge was spatially discretized using biased upwind differences with flux conserving formulation and Superbee flux limiter in the convective terms. Superbee flux limiter is a non-linear approximation tool switching between the high and low resolution schemes of flux formulation depending on the successive gradients of solutions, thus preventing nonphysical oscillation and numerical dispersion (Griffiths and Schiesser 2011). The model was solved by numerical method of lines (NMOL) using MATLAB's ODE solver for stiff system (Saucez et al. 2001; Schiesser and Griffiths 2009) and employing 151 spatial nodes and 1001–2001 time nodes for all simulation cases. Stability criteria were met by choosing the appropriate number of time nodes and solution convergence was achieved. The validity of the numerical model calculation was checked against an analytical solution of a simplified model describing isothermal and isobaric desorption of a binary Langmuirian gas mixture from an adsorbent column by purge with the less strongly adsorbed component of the mixture (Sircar and Kumar 1985; Sircar and Golden 1995).

Using a workstation of Quad 2.93 GHz Intel Core i3 530 @3575 MB, the computation (CPU) time for simulating a single purge case varied between 1–37 minutes; cases that included gas-solid heat transfer resistance in the model required the longest CPU times. The CPU time increased drastically to 5.5 hours when spatial nodes were increased from 151 to 251.

3.1 Conventional and pancake type adsorbers

Two adsorber designs having different length (L) to diameter (D) ratios but the same total amount of adsorbent [$W = (\pi/4)D^2L\rho_b \sim 160$ gms] packed in them were used in the simulations. They were (a) conventional type ($L =$ 8.38 cm, $D = 6.03$ cm, $L/D = 1.39$), and (b) pancake type ($L = 2.12$ cm, $D = 12$ cm, $L/D = 0.18$) configurations.

3.2 Ideal, hypothetical desorption process

The base case A for simulation was an idealized, hypothetical desorption process which is carried out under isothermal, isobaric, and local thermodynamic equilibrium conditions. This idealized case would require the least specific amount of purge gas for any specified desorption duty, thereby providing a benchmark for other realistic desorption conditions. Progressive simulations were carried out using more and more realistic situations by incorporating the effects of various mass, heat and momentum transfer resistances in the desorption model cases, and the results are compared vis a vis the desorption performance of the ideal process. These cases are defined by Table 2.

3.3 Effect of adsorbent particle size

Both adsorbate mass transfer (k_i) and gas-solid heat transfer (h) coefficients increase with decreasing d_p. Therefore, we studied the effects of lowering d_p (increasing transfer coefficients) on the desorption process for all cases B–F described by Table 2.

Figures 3, 4 and 5 show the simulation results for $d_p =$ 1500, 400 and 200 μm in adsorber $L/D = 1.39$, respectively. The variable f_1 is plotted against [$\bar{Q}_{O_2}/\bar{Q}^*_{O_2}$] where $\bar{Q}^*_{O_2}$ is the specific amount of O_2 purge gas needed to desorb 99.98 % of N_2 from the column [$f_1^* = 0.9998$] for the idealized case A. A full purge time, t_{purge}, of 2 seconds was used for all simulations except for the largest particle case where $t_{purge} = 10$ seconds was also used in order to evaluate the relative effect of mass transfer kinetics on faster cycle time. The corresponding mass fluxes of O_2 purge gas at the feed end, $Q_{O_2,\,feed}$, were, respectively, 5.35 and 1.07 mmoles/cm^2/s. All figures show the ideal desorption characteristics as a benchmark of the most efficient desorption by purge case.

Table 2 Legends for model assumptions used in various simulation cases

Legends	Model assumptions				
	Non-equilibrium thermodynamic (adsorption kinetics)	Mass axial dispersion in gas	Non-isobaric	Non-isothermal	Gas-solid heat transfer resistance
A					
B	Yes				
C	Yes	Yes			
D	Yes	Yes	Yes		
E	Yes	Yes	Yes	Yes	
F	Yes	Yes	Yes	Yes	Yes[a]

[a]With or without thermal axial dispersion in gas

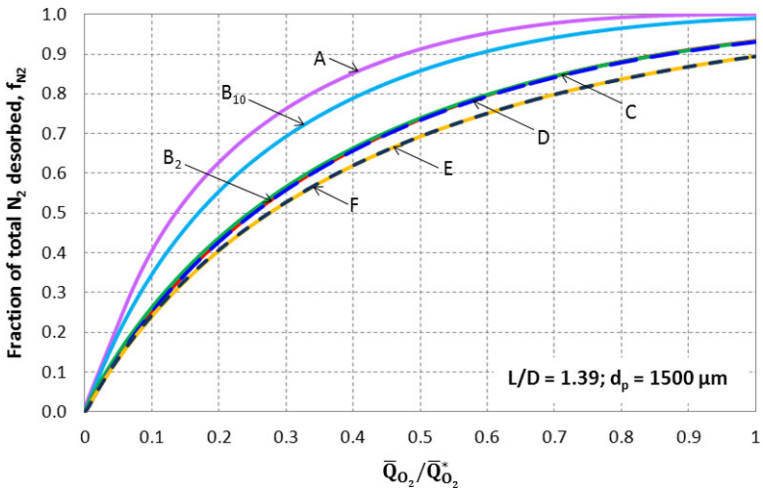

Fig. 3 Fraction of total N_2 desorbed vs amount of O_2 purge gas used. $L/D = 1.39$, $d_p = 1500$ µm, $k_{N_2} = 5.3\ s^{-1}$, $k_{O_2} = 5.1\ s^{-1}$, $Nu \sim 20.4$, $Re \sim 144$, $ha \sim 0.21$ cal/cm^3/s/K, $Q_{O_2,feed} = 5.35$, 1.07 mmoles/cm^2/s, respectively, for $t_{purge} = 2$, 10 s. Legends: Table 2

Curves B_{10} and B_2 in Fig. 3, with total desorption times of 10 and 2 seconds, respectively, show the detrimental effects of finite mass transfer kinetics on isothermal and isobaric desorption by purge using a relatively large adsorbent particle size ($d_p = 1500$ µm), which is typically used in a conventional O_2 PSA generator (Chai et al. 2011). Faster cycle time significantly increases the amount of O_2 purge gas needed for the same degree of N_2 desorption. Mass axial dispersion in gas phase (curve C) does not have much effect on the process. Column pressure drop (curve D) also does not appreciably add to the desorption inefficiency for the large particle case. Non-isothermal (adiabatic) operation substantially reduces desorption efficiency by purge (curve E). Finally, it was found that the inclusion of a finite gas-solid heat transfer resistance as well as gas phase heat axial dispersion in desorption by purge model does not have much impact on overall desorption efficiency (curve F). The reason for this interesting behavior will be discussed later.

Figure 4 shows that the detrimental effect of mass transfer kinetics on a rapid isothermal and isobaric desorption process using a relatively large adsorbent particle size can be substantially reduced by lowering d_p to 400 µm (curve B). At the same time, the desorption inefficiency of a non-isobaric process increases significantly due to increased column pressure drop (curve D). Adiabatic operation further lowers the desorption efficiency (curve E). The gas phase mass axial dispersion, and the gas-solid heat transfer resistance do not impact the desorption process.

Figure 5 demonstrates that the negative effect of finite mass transfer resistance on isobaric and isothermal desorption can be essentially eliminated by using an even smaller particle size of 200 µm, but the efficiency of isothermal, non-isobaric desorption substantially suffers due to higher column pressure drop. As expected, non-isothermal desorption further reduces the overall desorption efficiency.

Figures 6 and 7 plot the local total loading of N_2 (adsorbed + void) inside the column $[\bar{n}_{N_2}(z,t)]$ relative to the initial total N_2 loading $[N^0_{N_2}]$ as functions of dimensionless column distance (z/L) at the end of the purge desorption process when the fractions of total N_2 desorbed from the column were, respectively, 85 % ($f_{N_2} = 0.85$) and 90 % ($f_{N_2} = 0.90$). It should be noted that the durations of purge processes vary for these duties depending on particle sizes as well as model complexities. They show the locations of the trailing edges ($y_{N_2} < 0.0001$) of the proportionate patterned desorption fronts at the end of the purge process for dif-

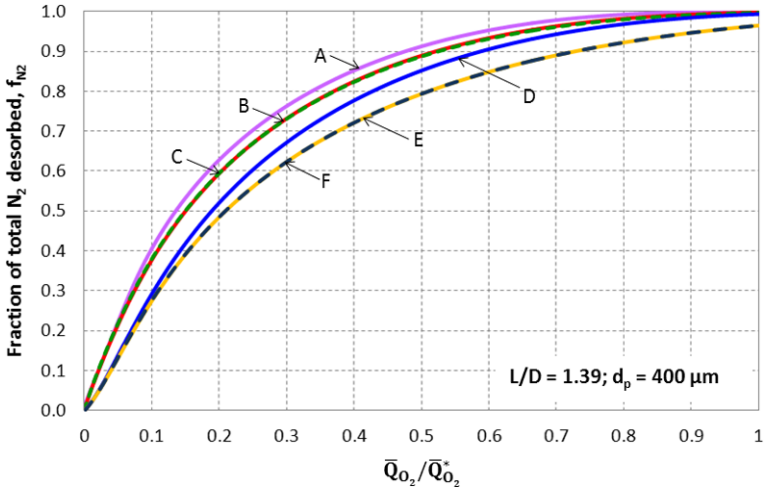

Fig. 4 Fraction of total N_2 desorbed vs amount of O_2 purge gas used. $L/D = 1.39$, $d_p = 400$ µm, $k_{N_2} = 73.8\ s^{-1}$, $k_{O_2} = 71.4\ s^{-1}$, $Nu \sim 10.3$, $Re \sim 38$, $ha \sim 1.49$ cal/cm^3/s/K, $Q_{O_2,feed} = 5.35$ mmoles/cm^2/s, $t_{purge} = 2$ s. Legends: Table 2

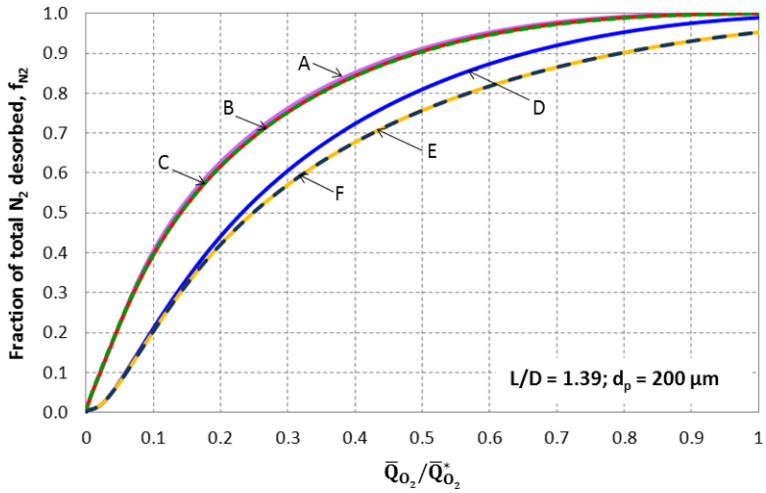

Fig. 5 Fraction of total N_2 desorbed vs amount of O_2 purge gas used. $L/D = 1.39$, $d_p = 200$ µm, $k_{N_2} = 295\ s^{-1}$, $k_{O_2} = 285\ s^{-1}$, $Nu \sim 7.5$, $Re \sim 19$, $ha \sim 4.3$ cal/cm^3/s/K, $Q_{O_2,feed} = 5.35$ mmoles/cm^2/s, $t_{purge} = 2$ s. Legends: Table 2

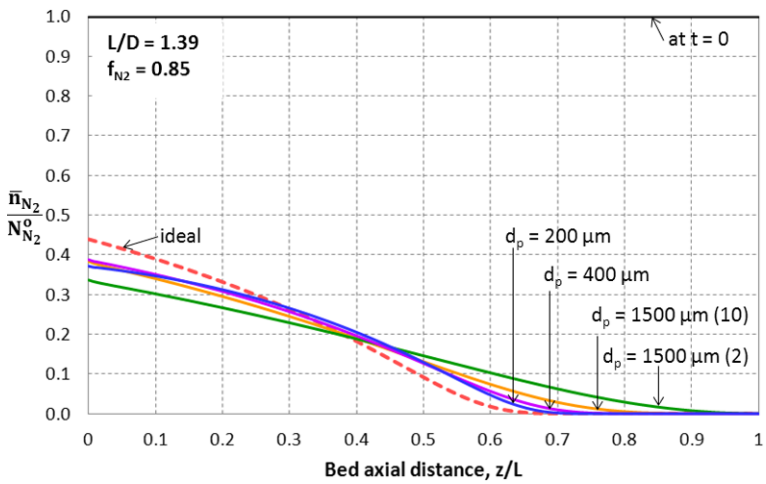

Fig. 6 Fraction of total N_2 loadings vs bed axial distance for $f_{N_2} = 0.85$. $L/D = 1.39$, $Q_{O_2,feed} = 5.35$, 1.07 (10) mmoles/cm^2/s, purge durations for achieving $f_{N_2} = 0.85$: 6 s, 1.68 s, 1.21 s, 1.33 s, and 0.80 s, respectively, for $d_p = 1500$ (10), 1500 (2), 400, 200 µm, and ideal case A. *Dashed line*: ideal case; *Solid lines*: case F (Table 2)

ferent adsorbent particle sizes and desorption times. Thus, these figures give the fractions (F) of the N_2-free adsorber volumes at the purge inlet end. The figures also provide the corresponding loading profiles for the idealized purge case A.

It may also be seen from Fig. 6 that a very small percentage of the column is free of N_2 ($F \sim 1$ %) when the adsorbent particle size is 1500 µm and the mass flux of O_2 purge gas, $Q_{O_2,feed}$, is high. Decreasing $Q_{O_2,feed}$ enlarges F to ~11 %. Reducing the adsorbent particle size for a rapid

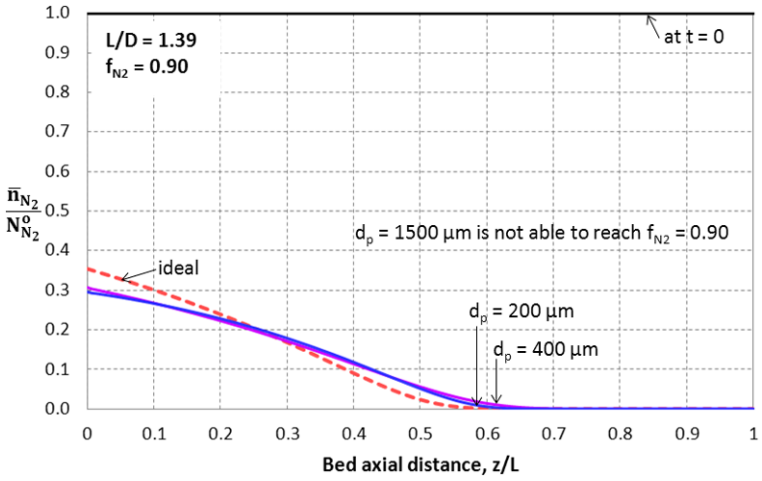

Fig. 7 Fraction of total N_2 loadings vs bed axial distance for $f_{N_2} = 0.90$. $L/D = 1.39$, $Q_{O_2,feed} = 5.35$ mmoles/cm^2/s, purge durations for achieving $f_{N_2} = 0.90$: 1.46 s, 1.59 s, and 0.95 s, respectively, for $d_p = 400$, 200 µm, and ideal case. *Dashed line*: ideal case A; *Solid lines*: case F (Table 2)

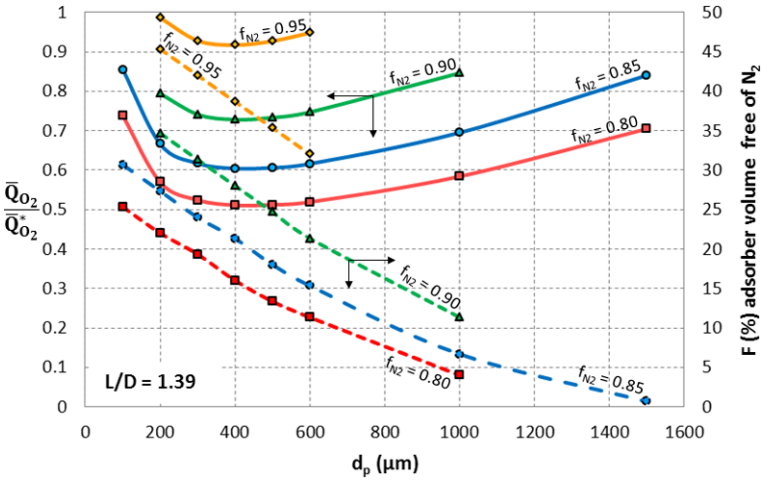

Fig. 8 Amount of O_2 purge required to desorb different fractions of total N_2 from a column (*solid lines*) and the corresponding fractional adsorbent volume free of N_2 at the purge inlet end (*dashed lines*) using different d_p. $L/D = 1.39$, $Q_{O_2,feed} = 5.35$ mmoles/cm^2/s, $t_{purge} \leq 2$ s, case F (Table 2)

purge process increases F; the model estimated values of F are, respectively, ~21 % and ~27 % for 400 and 200 µm particle sizes. The corresponding F value for the ideal purge case is ~30 %.

Figure 7 shows that a particle size of 1500 µm cannot achieve $f_{N_2} = 0.90$ in a rapid purge desorption situation using $Q_{O_2,feed} = 5.35$ mmoles/cm^2/s with $t_{purge} \leq 2$ s. On the other hand, smaller particle sizes of 400 and 200 µm can be used to achieve $f_{N_2} = 0.90$ and obtain, respectively, ~28 % and ~35 % N_2-free column fractions under identical conditions. The corresponding F value for the ideal purge case is ~37 %. Another interesting observation from Figures 6 and 7 is that the loading profiles for 400 and 200 µm particles are not very different in most of the column length for the fast desorption cases.

Figure 8 is a comprehensive summary of the simulated desorption performance data. It plots the dimensionless quantity of O_2 purge gas $[\bar{Q}_{O_2}/\bar{Q}^*_{O_2}]$ used in a rapid desorption process of $Q_{O_2,feed} = 5.35$ mmoles/cm^2/s with $t_{purge} \leq 2$ s as a function of adsorbent particle size $[d_p]$ for different extents of total N_2 desorption $[f_{N_2} =$ 0.8, 0.85, 0.9, 0.95] as well as the corresponding fractions of column volume free of N_2 at the purge inlet end $[F]$. It should be mentioned that larger particles cannot produce a positive value of F when f_{N_2} is low, and high f_{N_2} may not be achievable by very large or small particles.

A very important observation is that the purge gas requirement goes through a shallow minimum value for all values of f_{N_2}. The adsorbent particle size range where the minimum occurs is ~300–500 µm. The purge gas quantity for all values of f_{N_2} increases when $d_p < 300$ µm and when $d_p > 500$ µm, primarily due to detrimental effects of increased pressure drop and increased mass transfer resistance, respectively, as described earlier by Figs. 3–5. It may also be seen from Fig. 8 that F monotonically increases with decreasing d_p for all values of f_{N_2}. However, smaller d_p demands larger amount of O_2 purge.

An important finding of this analysis is that an optimum adsorbent particle size exists which will provide the best performance (lower BSF and higher O_2 recovery) by a MOC design if the RPSA cycle involves an explicit 'back purge with product gas' step.

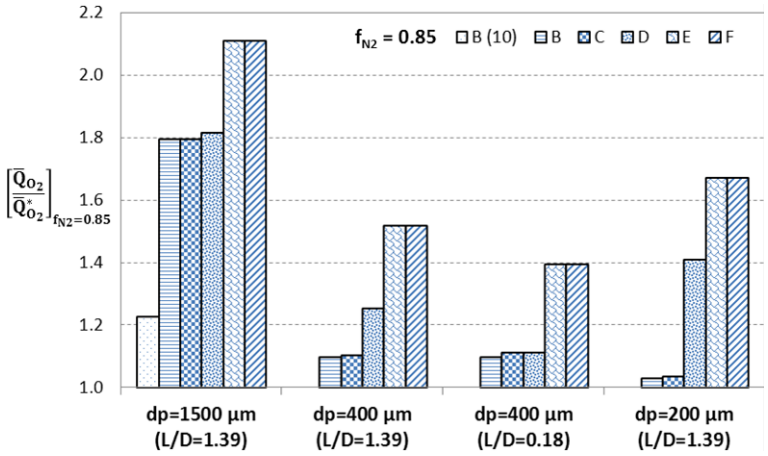

Fig. 9 Histograms showing the relative contributions of increase in O_2 purge gas amount due to different non-idealities (Table 2) for three different adsorbent particle sizes, $f_{N_2} = 0.85$, $L/D = 1.39, 0.18$. Base line = 1 (ideal case A)

A previous experimental and model study of a RPSA process for production of O_2 enriched air using a two step cycle (rapid column pressurization with air and rapid countercurrent depressurization of the column with continuous withdrawal of the product gas) has shown that the product O_2 purity can be maximized by using an optimum particle size (Alpay et al. 1994). This RPSA cycle does not contain an explicit and distinct 'product back purge step' but it implicitly uses a non-isobaric back purge with enriched O_2 gas during the depressurization step.

Figure 9 shows histograms describing progressive increases in O_2 purge gas quantities, or consequently, increases in inefficiency of the desorption process, above that for the idealized desorption case A (represented by base line = 1) due to inclusion of various non-idealities (B–F) listed in Table 2 using adsorbent particle sizes of 1500, 400 and 200 µm. The total fraction of N_2 desorbed from the adsorber for each case was 85 %, and the L/D ratio of the column was 1.39. Mass flux of O_2 purge gas introduced at the feed end, $Q_{O_2,\,feed}$, were, 5.35 and 1.07 mmoles/cm^2/s for $t_{purge} \leq 2$ s and $t_{purge} \leq 10$ s. The following conclusions can be drawn from the figure:

(a) Slow adsorption kinetics, column pressure drop, and non-isothermal desorption are the main causes of increased purge gas quantity for a specific desorption duty.
(b) Larger purge gas amount is required for a rapid desorption process than a conventional desorption process for the same extent of N_2 desorption.
(c) The gas phase mass axial dispersion does not affect the desorption efficiency.
(d) A finite heat transfer resistance between the gas and the solid does not have much effect on the overall desorption efficiency.
(e) The adverse effect of adsorption kinetics for a rapid desorption process can be significantly reduced by using smaller particle sizes, but at the cost of increased pressure drop, which eventually turns the desorption process inefficient below a certain particle size.

3.4 Pancake adsorber

PSA processes are often designed using a low L/D ratio which increases the column cross-sectional area and decreases the gas mass flux, and hence, column pressure drops. We simulated the desorption performance of a pancake ($L/D = 0.18$) adsorber containing the same amount of adsorbent as in the simulation cases above. This reduced the gas mass flux by a factor of ~4. The adsorbent particle size was 400 µm, $Q_{O_2,feed} = 1.35$ mmoles/cm^2/s, and $t_{purge} \leq 2$ s. Figure 10 shows the resulting plots of f_{N_2} vs $[\bar{Q}_{O_2}/\bar{Q}^*_{O_2}]$. A histogram of relative contributions of different non-idealities on the purge gas amount for the pancake adorber is also described in Fig. 9 which indicates that the detrimental effect of column pressure drop, and hence, the relative overall inefficiency of the purge process is decreased by using a pancake adsorber design compared to a common adsorber. The use of small particle size with a pancake adsorber design may lower purge gas amount but hydrodynamic problems like gas maldistribution, particle agglomeration, etc, can become serious problems (Porter et al. 1993; Moulijn and Van Swaaij 1976).

Figure 11 shows the plots of dimensionless total N_2 loadings vs distance in the column at the end of the purge desorption process when 85 % of N_2 was desorbed from the column. The figure compares these profiles for the ideal desorption case A and those for the common ($L/D = 1.39$) and pancake ($L/D = 0.18$) adsorber designs using the assumptions of Legend F in Table 2. It may be seen that use of a lower L/D reduces the fraction of N_2-free adsorber volume (F) at the purge inlet end. The values of parameter F were, respectively, 0.13 and 0.21 for L/D values of 0.18 and 1.39. The corresponding value of F for the ideal purge case was 0.3. This can be considered to be a negative characteristic of a pancake adsorber.

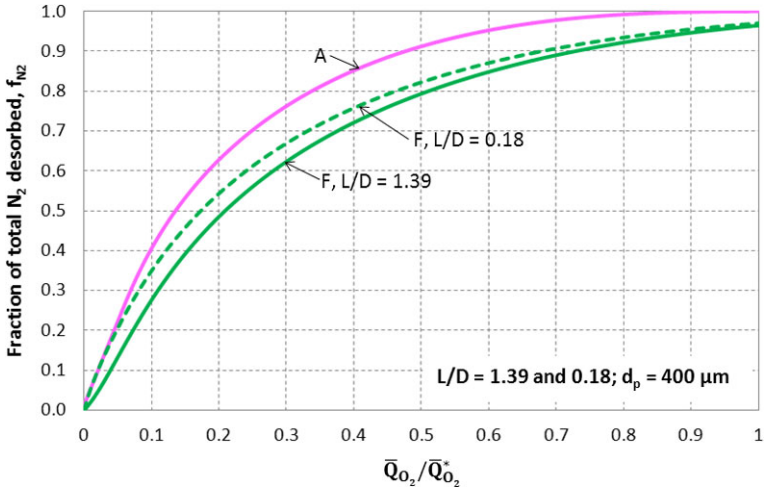

Fig. 10 Effects of column L/D on the efficiency of desorption of total N_2 by O_2 purge. $d_p = 400$ µm, $Q_{O_2,feed} = 1.35$ ($L/D = 0.18$), 5.35 ($L/D = 1.39$) mmoles/cm^2/s, $t_{purge} = 2$ s. Legends: cases A and F (Table 2)

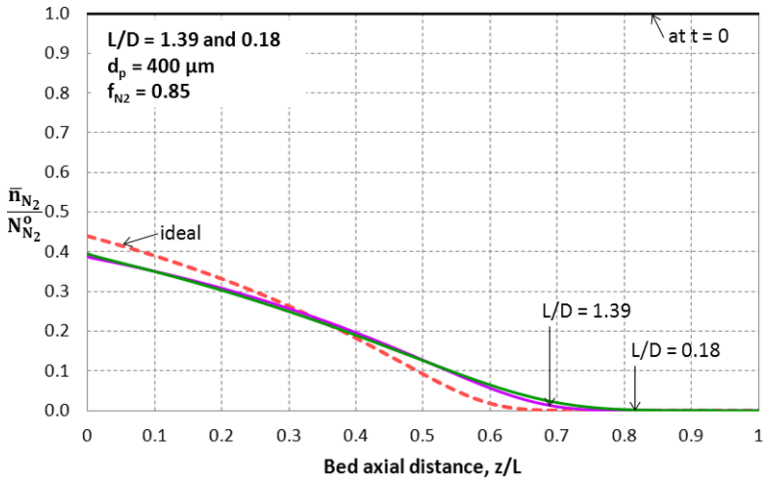

Fig. 11 Effects of column L/D on total N_2 loadings in column for $f_{N_2} = 0.85$. $d_p = 400$ µm, $Q_{O_2,feed} = 1.35$ ($L/D = 0.18$), 5.35 ($L/D = 1.39$) mmoles/cm^2/s, purge durations for achieving $f_{N_2} = 0.85$: 1.11 s, 1.21 s, and 0.80 s, respectively, for pancake adsorber, common adsorber, and ideal case. *Dashed line*: ideal case; *Solid lines*: case F (Table 2)

3.5 Non-isothermal column behavior for adiabatic desorption by purge

Figure 12 shows the simulated gas (dashed lines) and adsorbent (solid lines) temperature profiles as functions of dimensionless distance inside an adiabatic adsorber at the end of a rapid purge step for the case where the fraction of total N_2 desorbed from the column during the process was 0.85, the column L/D was 1.39, the adsorbent particle size was 400 µm, and the required duration of purge for achieving $f_{N_2} = 0.85$ was ~1.21 seconds. The values of gas-solid heat transfer coefficients (ha) used in the simulation were 1.49 (curve 2) and 0.53 (curve 3) cal/cm^3/s/K depending on the correlation used (see (23) or (24)). The figure also shows the temperature profiles for the case where instantaneous thermal equilibrium ($ha = \infty$) between the gas and the solid prevailed (curve 1). The profiles of gas phase mole fractions of N_2 in the column at the end of the purge process are also shown in the figure.

It may be seen from Fig. 12 that a sharp dip forms in both gas and solid phase temperature profiles near the purge gas inlet end of the column which reaches a minimum temperature difference (θ) of ~ -14.8 K, followed by a plateau region, and then both temperatures slowly increase towards the purge gas exit end. This is caused by self cooling of the adsorbent and gas in order to supply the endothermic heat of desorption of N_2 from the sensible heat of the gas and the solid during the purge process, since the purge gas inlet temperature is same as that of the initial column temperature. The entire column gets colder than the starting condition during the rapid purge process. An equilibrium theory for adiabatic desorption discusses the formation of a temperature plateau region (Sircar and Kumar 1985).

Three interesting observations from Fig. 12 are that (a) the gas temperature is slightly higher [more so when ha is smaller for obvious reasons] than the solid temperature at the purge gas inlet end until they reach their minimum plateau values, and then they become approximately equal for most of the remaining column length ($0 < z/L < 0.85$), (b) the existence of a minimum in the gas phase temperature profile means that heat flows by thermal axial dispersion in the gas phase towards the location of the temperature min-

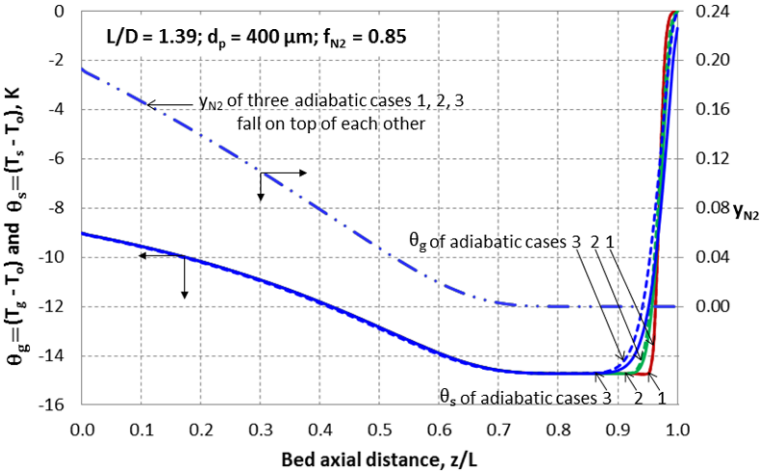

Fig. 12 Solid and gas temperature and gas phase N_2 mole fraction profiles in column at the end of purge extent $f_{N_2} = 0.85$. $L/D = 1.39$, $d_p = 400$ µm, $Q_{O_2,feed} = 5.35$ mmoles/cm^2/s, all required ~1.21 s of purge duration for achieving $f_{N_2} = 0.85$, gas-solid heat transfer coefficients (ha = cal/cm^3/s/K): ∞ (*curve 1*, equilibrium), 1.49 (*curve 2*, Wakao et al. 1979), 0.52 (*curve* 3, Kunii and Suzuki 1967)

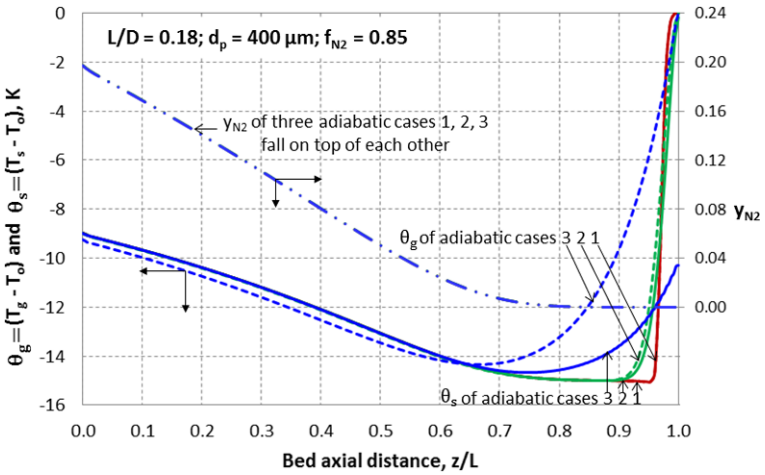

Fig. 13 Solid and gas temperature and gas phase N_2 mole fraction profiles in column at the end of purge extent $f_{N_2} = 0.85$. $L/D = 0.18$, $d_p = 400$ µm, $Q_{O_2,feed} = 1.35$ mmoles/cm^2/s, all required ~1.11 s of purge duration for achieving $f_{N_2} = 0.85$, gas-solid heat transfer coefficients (ha = cal/cm^3/s/K): ∞ (*curve 1*, equilibrium), 0.81 (*curve 2*, Wakao et al. 1979), 0.065 (*curve 3*, Kunii and Suzuki 1967)

imum from both ends of the column, and (c) the column temperature profiles for cases where ha has a finite value crisscrosses the corresponding profile for local thermal equilibrium case.

Figure 13 shows the column temperature profiles for the same desorption system employing a pancake adsorber ($L/D = 0.18$). The temperature profiles for the pancake adsorber are similar to those for the common adsorber when the gas-solid heat transfer coefficient is relatively large ($ha = 0.81$ cal/cm^3/s/K) except that the size of the plateau region is smaller. However, the differences between the gas and solid temperatures are relatively larger throughout the entire length of the column and a well-defined temperature plateau is not even formed when ha is sufficiently low ($ha =$ 0.065 cal/cm^3/s/K) for the pancake adsorber. In addition, the temperature minimum occurs at a location much deeper inside the column from the purge inlet end for the pancake adsorber. These complex temperature profiles, which are governed by the mass and heat transfer kinetics and the column pressure drop, determine the local adsorbate loadings during desorption, and hence the overall desorption characteristics of the column in a rapid, non-isothermal process. They can only be studied by a detailed non-isothermal, non-equilibrium, and non-isobaric desorption processes model. Experimental measurement of the profiles shown by Figs. 12 and 13 may be tedious and not even be practically feasible.

The simulations showed that the integrated overall N_2 desorption characteristics depicted by Figs. 3–5 and 9 were not affected appreciably by the presence of a finite gas-solid heat transfer resistance despite the differences in the gas and solid temperature profiles near the purge inlet section of the column when ha was low. This was because the gas and solid temperature profiles inside the column were not much different for most of the column length at the end of desorption process irrespective of the value of ha for all cases. This point is elaborated in the next section.

3.6 Parametric study of the effect of a finite gas-solid heat transfer coefficient

We parametrically simulated the effects of extreme values of gas-solid heat transfer coefficients ($ha = 0$, 0.21, and ∞ cal/cm^3/s/K) on the desorption process using an iden-

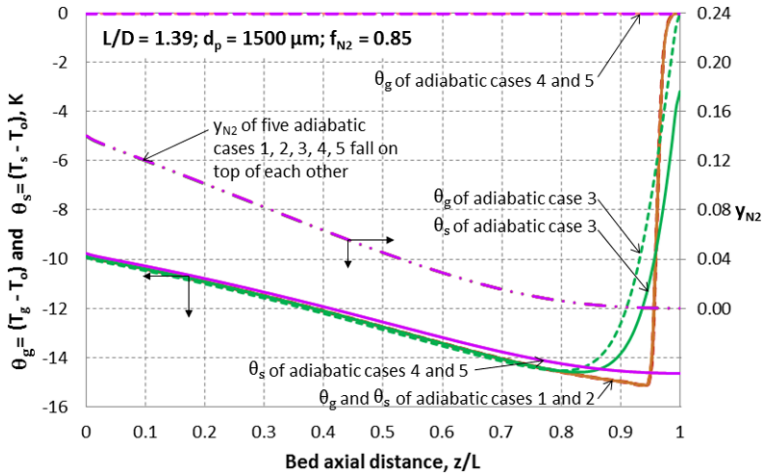

Fig. 14 Solid and gas temperature and gas phase N_2 mole fraction profiles in column at the end of purge extent $f_{N_2} = 0.85$. $L/D = 1.39$, $d_p = 1500$ µm, $Q_{O_2,feed} = 5.35$ mmoles/cm^2/s, all required ~1.68 s of purge duration for achieving $f_{N_2} = 0.85$, gas-solid heat transfer coefficients (ha = cal/cm^3/s/K): ∞ (*curves 1* and *2*, ignore and include thermal gas axial dispersion), 0.21 (*curve 3*, Wakao include thermal gas axial dispersion), 0 (*curves 4* and *5*, ignore and include thermal gas axial dispersion)

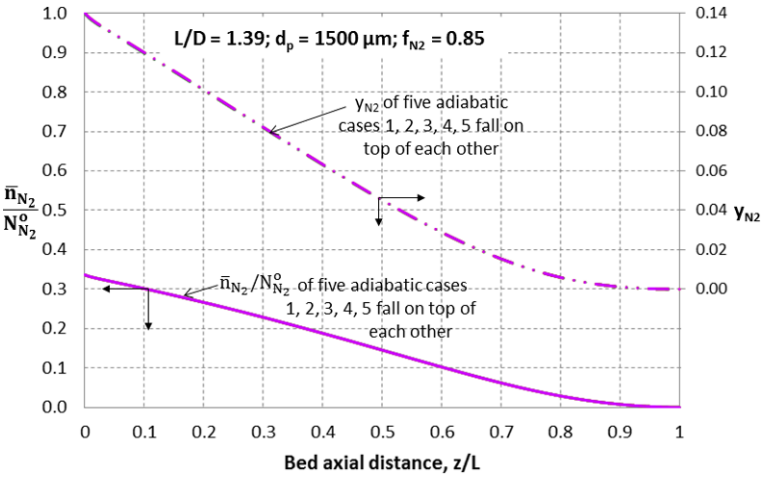

Fig. 15 Overlapping N_2 loadings (*solid lines*) and gas phase mole fraction (*dashed lines*) profiles in column at the end of purge extent $f_{N_2} = 0.85$. $L/D = 1.39$, $d_p = 1500$ µm, $Q_{O_2,feed} = 5.35$ mmoles/cm^2/s, required ~1.68 s of purge duration for achieving $f_{N_2} = 0.85$, for all cases of Fig. 14

tical system with $d_p = 1500$ µm whose overall performance is given by Fig. 3.

Figure 14 shows the gas and solid temperature profiles in the column at the end of the purge process of $f_{N_2} = 0.85$ using different values of ha for that system. It bears out a general observation of this study that the magnitude of a finite gas-solid heat transfer coefficient affects the gas and solid temperature profiles in the column only in the purge gas inlet section. The effect is small on the temperature profiles in the rest of the column. In fact, the gas and solid temperature profiles are practically independent of the value of ha in most of the column length at the end of the purge process. Furthermore, the N_2 loading profiles in the column for all of the adiabatic cases of Fig. 14 practically overlap on each other as shown by Fig. 15. As a consequence of this behavior, Fig. 16 shows that the overall integrated N_2 desorption profiles corresponding to different temperature profiles of Fig. 14 also overlap indicating that ha has practically no effect on these profiles for the present system.

It should, however, be emphasized here that the non-isothermal, non-isobaric, non-equilibrium desorption characteristics will generally be system specific, depending on adsorption equilibria and heats, mass and heat transfer kinetics, as well as the duration of the purge process.

4 Summary

Rapid pressure swing adsorption processes are frequently employed for production of ~90 % O_2 enriched gas from ambient air in medical oxygen concentrators for individual use. Many of these processes use a product gas back purge step as a part of the N_2 desorption scheme for cyclic regeneration of the N_2 selective adsorbent. A simple sensitivity analysis of an idealized RPSA process shows that any error in the estimation of the purge gas quantity can substantially magnify the errors in estimation of overall performance of the process such as bed size factor (BSF) and O_2 recovery (R).

A detailed mathematical simulation of a rapid, adiabatic, non-isothermal, non-isobaric, and non-equilibrium desorption process for N_2 removal from a LiX zeolite column,

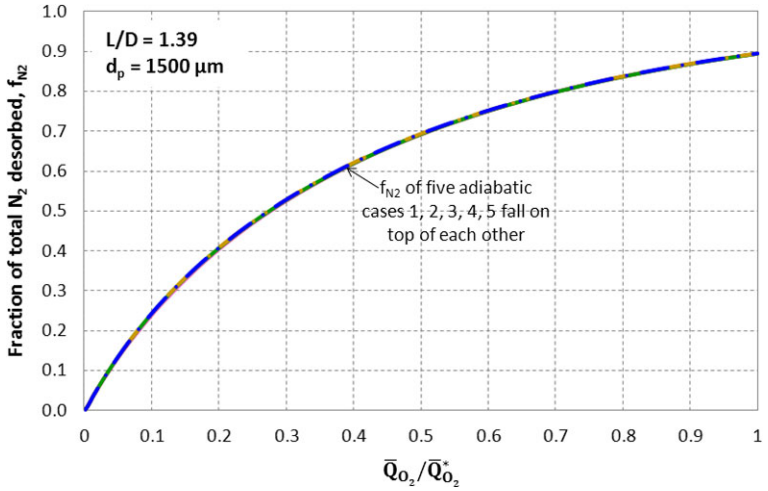

Fig. 16 Fraction of total N_2 desorbed vs purge O_2 quantity for all cases of Fig. 14

which is initially equilibrated with air, by pure O_2 purge is presented. Coupled partial differential equations describing mass balances, gas and solid phase heat balances, and pressure drop in the column were simultaneously solved numerically in conjunction with published models for describing binary adsorption equilibria for the system and conventional linear driving force model for adsorption kinetics. Ergun equation described the transient column pressure drop. Effects of relatively short and long desorption time, adsorbate mass transfer coefficient, column pressure drop, column non-isothermality, gas-solid heat transfer coefficient, mass and heat axial dispersions in gas phase, adsorbent particle size, and column geometry (length to diameter, L/D, ratio) on desorption efficiency by purge were systematically evaluated.

The minimum amount of O_2 purge gas for a given desorption duty (fraction of total N_2 that is initially present in the column removed by the purge process) is needed by an idealized case where the process is isothermal, isobaric, and controlled by local thermodynamic equilibrium. A realistic desorption by purge process requires a significantly larger purge gas quantity for the same duty. The analysis shows that adsorption kinetics (especially for a rapid desorption process), column pressure drop, and non-isothermal column operation, are major contributors to desorption inefficiency. The influence of gas phase mass and thermal axial dispersions is minimal. Lowering adsorbent particle size increases adsorption kinetics but at the cost of increased pressure drop. Consequently there is an optimum particle size which can minimize the purge gas requirement for a specific desorption duty. A pancake shaped column ($L/D < 0.2$) can be effective in lowering the effect of column pressure drop in conjunction with smaller adsorbent particles, but chances of gas mal-distribution increase. The negative impact of non-isothermal operation cannot generally be avoided, and needs to be accounted for in a realistic process design. This work incorporates some of the details of a complex subject which are often ignored by the published literature. The critical comparative results of various transfer resistances on the desorption by purge process, albeit for a simple model system, as shown by the histograms of Fig. 9, are very instructive.

The gas and solid temperature profiles in the column at the end of a rapid desorption process can be complex and non-intuitive. They dip to a minimum value near the purge gas inlet end of the column to form a plateau region, and then slowly rise towards the exit end. The entire column cools down to supply the heat of desorption if the purge gas is not heated above the initial column temperature. Existence of a finite gas-solid heat transfer coefficient creates different gas and solid temperature profiles inside the column which are substantially different from those of a column operating under local thermal equilibrium condition only in a section near the purge gas inlet end. These profiles are very similar in the balance of the column length irrespective of the value of the heat transfer coefficient. Consequently, the influence of finite heat transfer coefficient on an integrated overall desorption efficiency is small for the present system.

A very important conclusion of this study is that a simplified isothermal, or isobaric, or local equilibrium process design model of rapid desorption can lead to an unrealistically optimistic MOC process performance.

References

Alpay, E., Kenney, C.N., Scott, D.M.: Adsorbent particle size effects in the separation of air by rapid pressure swing adsorption. Chem. Eng. Sci. **49**, 3059 (1994)

Basmadjian, D., Ha, K.D., Pan, C.Y.: Nonisothermal desorption by gas purge of single solutes in fixed-bed adsorbers. I. Equilibrium theory. Ind. Eng. Chem. Process Des. Dev. **14**, 328 (1975a)

Basmadjian, D., Ha, K.D., Proulx, D.P.: Nonisothermal desorption by gas purge of single solutes from fixed-bed adsorbers. II. Experimental verification of equilibrium theory. Ind. Eng. Chem. Process Des. Dev. **14**, 340 (1975b)

Chai, S.W., Kothare, M.V., Sircar, S.: Rapid pressure swing adsorption for reduction of bed size factor of a medical oxygen concentrator. Ind. Eng. Chem. Res. **50**, 8703 (2011)

Dhingra, S.C., Gunn, D.J., Narayanan, P.V.: The analysis of heat transfer in fixed beds of particles at low and intermediate Reynolds numbers. Int. J. Heat Mass Transf. **27**, 2377 (1984)

Ergun, S.: Fluid flow through packed columns. Chem. Eng. Prog. **48**, 89 (1952)

Griffiths, G.W., Schiesser, W.E.: Traveling Wave Analysis of Partial Differential Equations: Numerical and Analytical Methods with Matlab and Maple. Academic Press, San Diego (2011). Chap. 2

Jacob, P., Tondeur, D.: Non-Isothermal gas adsorption in fixed beds. II. Non-linear equilibrium theory and 'Guillotine' effect. Chem. Eng. J. **26**, 41 (1983)

Kopaygorodsky, E.M., Guliants, V.V., Krantz, W.B.: Predictive dynamic model of single-stage ultra-rapid pressure swing adsorption. AIChE J. **50**, 953 (2004)

Kumar, R., Sircar, S.: Adiabatic sorption of bulk single adsorbate from an inert gas—effect of gas-solid mass and heat transfer coefficients. Chem. Eng. Commun. **26**, 319 (1984a)

Kumar, R., Sircar, S.: Adiabatic sorption of dilute single adsorbate from an inert gas—effect of gas-solid mass and heat transfer coefficients. Chem. Eng. Commun. **26**, 339 (1984b)

Kunii, D., Suzuki, M.: Particle-to-fluid heat and mass transfer in packed beds of fine particles. Int. J. Heat Mass Transf. **10**, 845 (1967)

Langer, G., Roethe, A., Roethe, K.P., Gelbin, D.: Heat and mass transfer in packed beds. III. Axial mass dispersion. Int. J. Heat Mass Transf. **21**, 751–759 (1978)

Moulijn, J.A., Van Swaaij, W.P.M.: The correlation of axial dispersion data for beds of small particles. Chem. Eng. Sci. **31**, 845 (1976)

Porter, K.E., Ali, Q.H., Hassan, A.O., Aryan, A.F.: Gas distribution in shallow packed beds. Ind. Eng. Chem. Res. **32**, 2408 (1993)

Rama Rao, V., Farooq, S., Krantz, W.B.: Design of a two-step pulsed pressure swing adsorption based oxygen concentrator. AIChE J. **56**, 354 (2010)

Rege, S.U., Yang, R.T.: Limits for air separation by adsorption with LiX zeolite. Ind. Eng. Chem. Res. **36**, 5358 (1997)

Rhee, H.K., Amundson, N.R.: An analysis of an adiabatic adsorption column. Part I. Theoretical development. Chem. Eng. J. **1**, 241 (1970)

Rhee, H.K., Heerdt, E.D., Amundson, N.R.: An analysis of an adiabatic adsorption column. Part III. Adiabatic adsorption of two solutes. Chem. Eng. J. **3**, 22 (1972)

Ruthven, D.M.: Principles of Adsorption and Adsorption Processes. Wiley, New York (1984)

Santos, J.C., Portugal, A.F., Magalhaes, F.D., Mendes, A.: Simulation and optimization of small oxygen pressure swing adsorption units. Ind. Eng. Chem. Res. **43**, 8328 (2004)

Santos, J.C., Portugal, A.F., Magalhaes, F.D., Mendes, A.: Optimization of medical PSA units for oxygen production. Ind. Eng. Chem. Res. **45**, 1085 (2006)

Saucez, P., Schiesser, W.E., Wouwer, A.V.: Upwinding in the method of lines. Math. Comput. Simul. **56**, 171 (2001)

Schiesser, W.E., Griffiths, G.W.: A Compendium of Partial Differential Equation Models: Method of Lines Analysis with Matlab. Cambridge University Press, Cambridge (2009)

Schiesser, W.E.: PDE boundary conditions from minimum reduction of the PDE. Appl. Numer. Math. **20**, 171 (1996)

Sircar, S.: Influence of gas-solid heat transfer on rapid PSA. Adsorption **11**, 509 (2005)

Sircar, S., Golden, T.C.: Isothermal and isobaric desorption of carbon dioxide by purge. Ind. Eng. Chem. Res. **34**, 2881 (1995)

Sircar, S., Kumar, R.: Equilibrium theory for adiabatic desorption of bulk binary gas mixtures by purge. Ind. Eng. Chem. Process Des. Dev. **24**, 358 (1985)

Sircar, S., Myers, A.L.: Gas separation by zeolites. In: Auerbach, S.M., Carrado, K.A., Dutta, P.K. (eds.) Handbook of Zeolite Science and Technology, pp. 1063–1105. Dekker, New York (2003). Chap. 22

Sircar, S., Rao, M.B., Golden, T.C.: Fractionation of air by zeolites. In: Dabrowski, A. (ed.) Adsorption and Its Applications in Industry and Environmental Protection, vol. 120, Part 1, pp. 395–423. Elsevier, New York (1999)

Skarstrom, C.W.: Method and apparatus for fractionating gaseous mixtures by adsorption. U.S. patent 2,944,627 (1960)

Todd, R.S., Webley, P.A.: Mass-transfer models for rapid pressure swing adsorption simulation. AIChE J. **52**, 3126 (2006)

Wakao, N., Kaguei, S., Funazkri, T.: Effect of fluid dispersion coefficients on particle-to-fluid heat transfer coefficients in packed beds. Chem. Eng. Sci. **34**, 325 (1979)

Wicke, E.: Empirische and teoretische Untersuchungen der Sorptionsgeschwindigkeit von Gasen an porösen Stoffen I. Kolloid Z. **86**, 167 (1939a)

Wicke, E.: Empirische and teoretische Untersuchungen der Sorptionsgeschwindigkeit von Gasen an porösen Stoffen II. Kolloid Z. **86**, 295 (1939b)

Zhong, G.M., Rankin, P.J., Ackley, M.W.: High frequency PSA process for gas separation. U.S. patent 7,828,878 (2010)